Valley Carrier Dynamics in Monolayer Molybdenum Disulfide from Helicity-Resolved Ultrafast Pump–Probe Spectroscopy

Qinsheng Wang,[†,§] Shaofeng Ge,[†,§] Xiao Li, Jun Qiu,[§] Yanxin Ji,[§] Ji Feng,[§,∥] and Dong Sun[§,∥,*]

[§]International Center for Quantum Materials, Peking University, Beijing 100871, China, and [∥]Collaborative Innovation Center of Quantum Matter, Beijing, 100871, China. [†]These authors contributed equally to this work.

ABSTRACT We investigate the valley-related carrier dynamics in monolayer molybdenum disulfide using helicity-resolved nondegenerate ultrafast pump–probe spectroscopy at the vicinity of the high-symmetry K point under the temperature down to 78 K. Monolayer molybdenum disulfide shows remarkable transient reflection signals, in stark contrast to bilayer and bulk molybdenum disulfide due to the enhancement of many-body effect at reduced dimensionality. The helicity-resolved ultrafast time-resolved result shows that the valley polarization is preserved for only several picoseconds before the scattering process makes it undistinguishable. We suggest that the dynamical degradation of valley polarization is attributable primarily to the exciton trapping by defect states in the exfoliated molybdenum disulfide samples. Our experiment and a tight-binding model analysis also show that the perfect valley circular dichroism selectivity is fairly robust against disorder at the K point but quickly decays from the high-symmetry point in the momentum space in the presence of disorder.

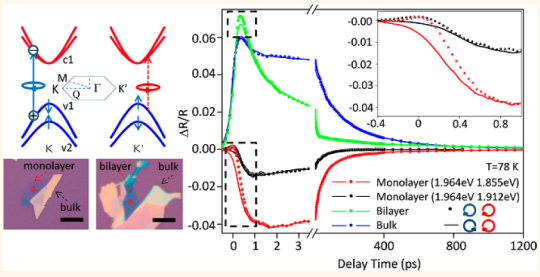

KEYWORDS: molybdenum disulfide · transition-metal dichalcogenides · ultrafast spectroscopy · valley carrier dynamics · disorder

Molybdenum disulfide (MoS_2) as a representative of the most explored two-dimensional (2D) transition-metal dichalcogenides (TMDC) has been shown to exhibit remarkable optical properties during the past few years. These include the transition from indirect to direct band gap when reaching monolayer from bulk,[1,2] trion state with large bonding energy,[3,4] efficient valley and spin control by optical helicity,[5−7] and signature of coherence[8] between the two valleys due to its valley-selective circular dichroism (CD).[5,9] These unique optical properties, as well as emergence of convenient and controllable growth methods to acquire the monolayer materials, make this category of materials especially interesting and promising for possible valleytronics applications.[10−13]

Toward the application of TMDC in future valleytronics, it is critical to examine the dynamics of incipient valley polarization by CD and the subsequent relaxation dynamics, especially various scattering channels that can degrade the valley polarization. Previous photoluminescence (PL) measurement relies on the photon emission process to read out valley carrier distribution, which only gives partial information about the valley degree of freedom even when time-resolved PL measurement is performed.[14,15] This is because the scattering of carriers to a nonradiative state cannot be detected in PL measurement. As a powerful tool for studying the various dynamics in materials and devices, ultrafast pump–probe spectroscopy has been applied to study thin layer and bulk MoS_2 recently.[16−19] However, existing experiments have not addressed the interesting valley dynamics due to two factors: (1) the lack of helicity resolution and (2) large pump photon energy that is far away from the transition at the vicinity of K point. A helicity-resolved ultrafast pump–probe experiment on monolayer MoS_2 with transitions at the vicinity of K point is highly desirable to resolve the valley-related carrier dynamics, in the aims of both understanding the discrepancies in existing measurements, such as the variation of valley polarization from

* Address correspondence to sundong@pku.edu.cn.

Received for review September 12, 2013 and accepted November 13, 2013.

Published online November 13, 2013
10.1021/nn405419h

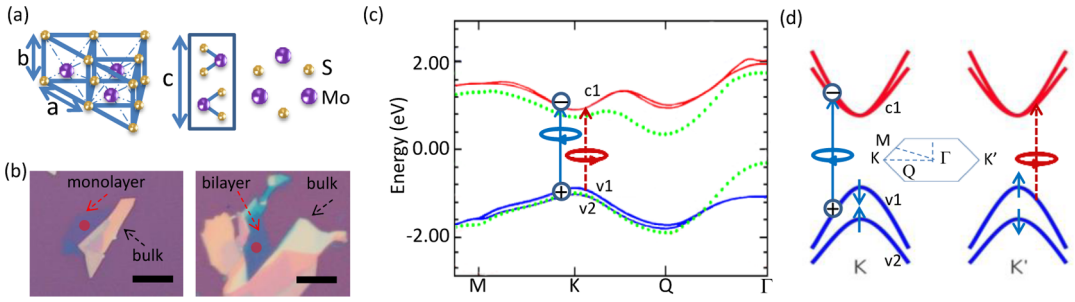

Figure 1. (a) Lattice structure of MoS_2. (b) Optical micrograph of MoS_2 on 285 nm SiO_2. The red spot marks the probe position in spectroscopy measurement. Scale bar: 10 μm. (c) Band diagram of monolayer (solid) and bulk (dash) MoS_2 and pump (blue) probe (red) photon transition configuration. (d) Lowest-energy conduction bands and the highest-energy valence bands, with valley selection rule for circular polarized light.

30 to 100% in different experiments,[5−7,20] and stepping toward future valleytronics applications, such as optical initialization and manipulation of the valley degree of freedom and coherence in TMDC.[8]

In this article, we present a helicity-resolved optical nondegenerate pump−probe experiment on exfoliated monolayer MoS_2 in a reflection setup. Figure 1a shows the lattice structure of MoS_2, which has a hexagonal crystal structure with covalently bonded S−Mo−S. *Ab initio* band structure results[21−25] (Figure 1c) indicate that MoS_2 crosses over from an indirect gap semiconductor with a multilayer to a direct gap semiconductor with a monolayer. Because the two sublattices are occupied by one molybdenum and two sulfur atoms, respectively, inversion symmetry is broken in the monolayer MoS_2. The broken inversion symmetry, together with the broken spin degeneracy by spin−orbit coupling, leads to valley-dependent optical selection rules for interband transitions at K and K′ points: interband transitions at K (K′) valleys are allowed for optical excitation of left (right) circular polarized light only.[5,6,9]

As shown in Figure 1d, valley polarized carriers are injected by left/right (σ^-/σ^+) circular polarized pump pulse and detected by measuring the differential reflection of the left circular (σ^-) probe pulse. Except in pump-wavelength-dependent measurements, the pump and probe photon energies are centered at 1.964 and 1.912 eV, respectively, with a 4 meV bandwidth, which is to be compared with the A exciton energy[1,2] centered at 1.86 eV with 70 meV bandwidth from PL measurement (see Supporting Information). Both pump and probe photon-excited transitions are from the highest valence band v1 to lowest conduction band c1 at the vicinity of K point (Figure 1c). The transition between spin−orbital interaction split valence band v2 and c1 is not directly excited by one-photon absorption in a monolayer. Under perfect circular polarized valley selection,[5,9] the σ^+ pump photon excites carriers into the K′ valley only, while the σ^- probe photon is sensitive to pump-induced carrier distribution change in the K valley. Thus, intervalley scattering of carriers between K and K′ can be dynamically measured by varying the pump and probe photon delays. Here we measure the change of the probe pulse reflection, ΔR, induced by the pump. ΔR is then normalized by the probe reflection to obtain the differential reflection, $\Delta R/R = (R' - R)/R$, where R' and R are the reflection of the probe pulse from the sample with and without the presence of the pump pulse, respectively.

RESULTS AND DISCUSSION

Figure 2 shows a representative helicity-resolved transient reflection spectra of monolayer, bilayer, and bulk MoS_2 at 78 K. The monolayer shows negative ΔR except at the vicinity of time zero. In contrast, both bilayer and bulk show positive ΔR during the entire course of the measurements. A remarkable observation is that the initial transient reflection spectra of the monolayer are different with σ^+ and σ^- pump excitations. The difference is observable over a period of about 1 ps. This difference varies on different places of one sample and on different samples. A large variation from 1 to 7 ps is observed on different samples (see Supporting Information). In contrast, the transient reflection of bulk is independent of pump helicity. If the pump photon energy increases slightly to 2.072 eV (moving the pump photon excitations by 212 meV away from the K point), the pump helicity dependence completely disappears (Figure 2b). The temperature-dependent measurements show that the pump helicity dependence of ΔR on the monolayer persists up to 298 K (Figure 3a). In contrast to the full negative ΔR over entire delays for σ^+ pump excitation at 78 K, the ΔR turns positive at the vicinity of time zero at 298 K. Figure 3b shows that the positive ΔR component also increases with temperature for σ^- pump excitation. The pump helicity dependence of transient reflection is also observed in the bilayer due to the broken inversion symmetry by coupling to the substrate,[6,26] which disappears at room temperature in the as-prepared sample (see Supporting Information).

The decay from the negative peak of ΔR shown in Figure 3c is multiexponential with two distinct time scales, namely, a fast component (τ_1) of 7.1 ps and a slow component (τ_2) of 61.3 ps at 78 K. Both τ_1 and τ_2

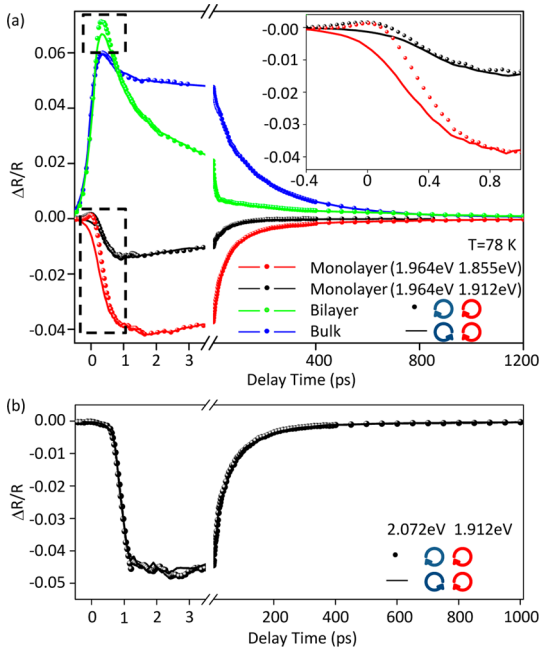

Figure 2. (a) Helicity-resolved transient reflection dynamics at 78 K on monolayer (black and red), bilayer (green), and bulk MoS_2 (blue). The pump photon is set at 1.964 eV (633 nm) for all curves in the figures. The probe photon energy is set at 1.855 eV (650 nm) for comparison of transient reflection dynamics of samples with different thickness. For monolayer, probe photon energy of 1.912 eV (670 nm) is measured for comparison. The inset shows the signal at the vicinity of time zero of the monolayer. (b) Helicity-resolved transient reflection dynamics of monolayer MoS_2 with pump photon energy of 2.072 eV (600 nm) and probe photon energy of 1.912 eV (650 nm) at 77 K. The lines and dots show results from cross- and co-circular pump−probe polarization configurations in all figures.

increase with temperature, indicating a phonon-related process during both decays (Figure 3d). According to the previous studies,[14,16] we attribute the fast decay to phonon scattering and the slow decay to nonradiative interband electron−hole recombination. The slow component is much faster in the monolayer than in the bulk due to the transition from direct band gap to indirect band gap.[1,2,16]

We now turn to the interpretation of the sign of the transient reflection signal observed in the experiment. The positive ΔR of bulk and bilayer is consistent with the free carrier or exciton state-filling effect as studied previously in the literature.[16−18] The pump-induced free carriers or excitons occupy the probe transition states and reduce the probe photon absorption. Thus the Pauli blocking enhances the probe reflection, leading to a positive ΔR. As carrier occupation effect dominates ΔR at moderate carrier excitation intensities, many-body effects become significant in semiconductors with reduced dimensionalities or at high carrier excitation intensities.[27−33] In the case of highly excited (typical pump photon fluence of $4 \times 10^{14}/cm^2$) two-dimensional monolayer MoS_2, the contribution of many-body effects to ΔR cannot be neglected, though the initial positive ΔR can be dominated by an instantaneous exciton ground-state bleaching.[34] Because we use probe photon energy equivalent to the exciton transition at the band edge, the band gap renormalization effect due to the Coulomb interactions of the dense electron−hole plasma contributes to the negative ΔR signal[28,30−33] and matches the sign of ΔR in the monolayer that we measured. Here we rule out the possibility that the negative sign of ΔR of the monolayer is from a resonant transition of the probe, as observed by similar experiment in GaAs,[35] since the probe photon energy is close to the resonance of A exciton in the bilayer and bulk, too. The monolayer sample also shows the same ΔR sign when we switch the probe wavelength to nonresonant 633 nm (see Supporting Information), which further rules out the resonant transition effect. The argument that the band gap renormalization may dominate the ΔR signal is also supported by the decrease of positive ΔR at the vicinity of time zero with decreasing temperature, as measured in Figure 3b, which matches temperature dependence of the band gap renormalization effect.[28,32]

As to the helicity-resolved results on the monolayer, the independence of pump helicity when pumping with 600 nm is in good agreement with previous PL excitation measurement.[15,36] However, from our dynamics measurement, an initial valley carrier polarization by the excitation is not observed within the ~200 fs time resolution (Figure 2b). Thus, the absence of the valley polarized CD is not attributable to the phonon-assisted intervalley scattering when carriers relax from relatively high excited states,[36] as the carrier phonon scattering time scale is larger than 200 fs. The only interpretation would be that the valley CD selectivity decays quickly when the excitation is away from the vicinity of the high symmetry K point, and thus 600 nm σ^- pump excites carriers almost equally in K and K′ valleys initially. For a perfect crystal without disorder, theoretical calculations predict near unity valley CD selectivity over almost the whole K and K′ valleys.[5,9] However, in an exfoliated MoS_2 sample with significant disorder, the valley CD selectivity decays due to the presence of disordered defects. A tight-binding simulation of valley CD selectivity as a function of disorder strength W, which is an additive onsite energy perturbation akin to Anderson disorder, is shown in Figure 4 (simulation details in Supporting Information). When there is no disorder ($W = 0$ eV), the valley CD selectivity at K is 1. We choose a small region around K in which the valley CD selectivity is larger than 98.5%. Upon the introduction of disorder, the valley CD selectivity decreases. The valley CD selectivity at K decreases to 80% when $W = 0.6$ eV, while valley CD selectivity away from the K point decreases, by a much greater amount, down to 20% (Figure 4b). Therefore, disorder has a pronounced effect on the valley CD selectivity for off-resonance transitions, but the

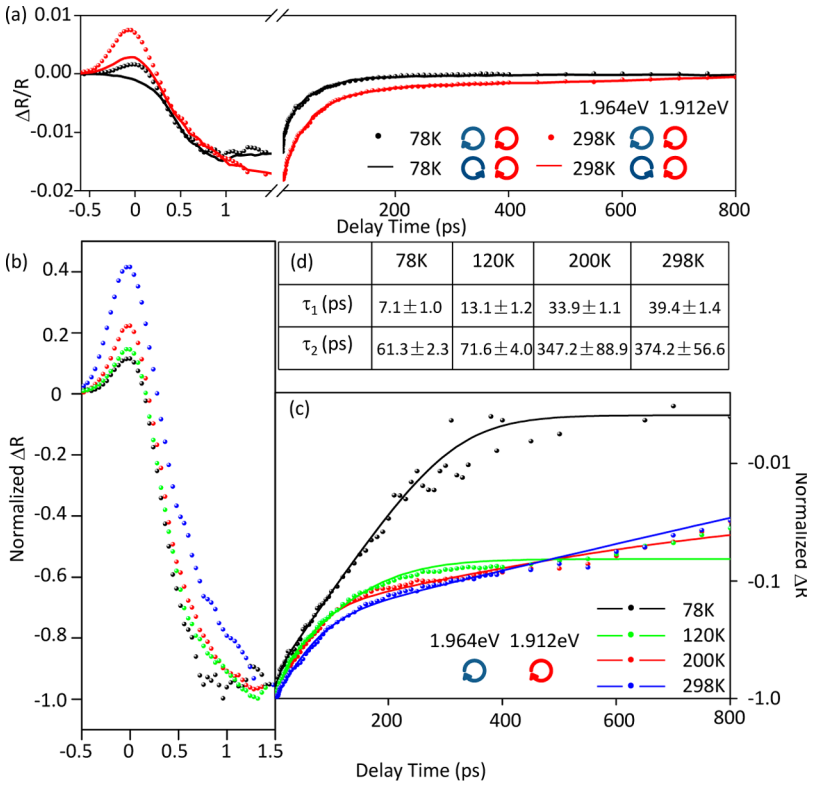

Figure 3. Temperature dependence of helicity-resolved transient reflection dynamics of monolayer MoS_2 with a pump wavelength of 633 nm and a probe wavelength of 650 nm. (a) Transient reflection dynamics of monolayer at 78 K (red) and 298 K (black) with cross- (line) and co-circular (dot) polarized pump−probe configurations. (b) Evolution of transient reflection dynamics at vicinity of time zero with temperature from 298 to 78 K measured with co-circular pump−probe polarization configuration. (c) Two exponential decay function of $A\cdot\exp(-t/\tau_1) + B\cdot\exp(-t/\tau_2)$ fitting of transient reflection decay tails from the negative peak at different temperatures. (d) Fitting parameters, fast (τ_1) and slow (τ_2) decay time constant for decay curves in panel c.

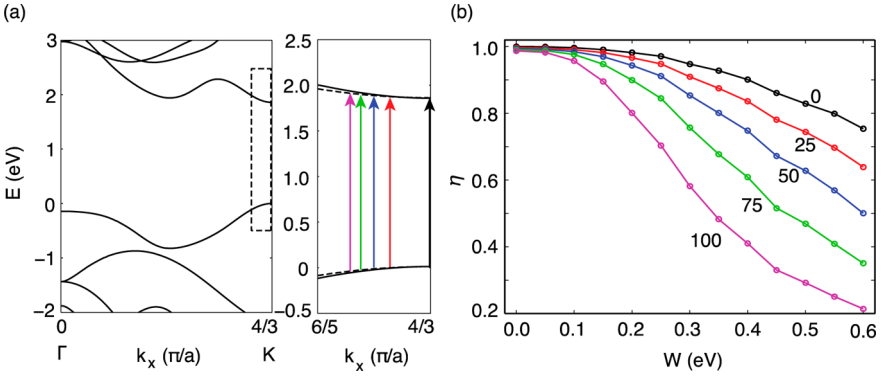

Figure 4. (a) Left: Band structure of MoS_2 monolayer along Γ→K from density functional theory (DFT) calculations. There is a direct gap of 1.86 eV at K point from the simulation. Right: Zooming into the region bounded by dashed lines in the left panel. The bands based on DFT are shown by solid line, and the ones from the tight-binding (TB) calculation are shown by dashed line. The vertical arrows with different colors represent the optical transitions, where the transition energy is 1.860, 1.885, 1.910, 1.935, and 1.960 eV as we move away from K, respectively. (b) Optical selectivity (η) decays with disorder (W). Every colored line corresponds to the transitions with the same color in (a). The numbers near lines show the transition energy relative to the direct band gap.

on-resonance transition at the high symmetry K point is fairly robust against disorder. As a result, when pumping closer to the K point at 633 nm, the valley polarization can still be created.

The valley polarization excited by 633 nm is only preserved for several picoseconds before the scattering process makes the carrier distributions in K and K′ valleys equivalent. We attribute the dominant mechanism of this fast scattering to the trapping of exciton by defects. The trapped exciton (or localized exciton) has been observed to emit at 1.8 eV with no valley CD selectivity.[6,15] For the monolayer with significant surface-to-volume ratios, the surface defects can act as exciton traps, and this trapping process can be very efficient.[37] The efficient exciton trapping can account for the very short A exciton emission

lifetime[14,15] and low PL quantum yield observed on monolayer MoS_2.[6,8,14,15] In previous ultrafast differential transmission measurement on a suspended MoS_2 sample and time-resolved PL measurement,[14−16] the scattering time is observed to be 2−4 ps. This matches the several picoseconds scattering time measured in our experiment considering it can vary from sample to sample with different disorder strengths. Here we cannot fully rule out the possibility that optical phonon scattering can contribute to the intervalley scattering process, considering its probable picosecond time scale. However, we infer that an optical phonon scattering dominated intervalley scattering process is unlikely for at least two reasons: First, optical phonon scattering may have stronger temperature dependence compared to the weak temperature dependence from 78 to 298 K observed in our experiment (Figure 3a). Second, the intervalley phonon scattering time should not have large variation on different samples, especially on different spots on one sample as observed in the sample-dependent measurement (Supporting Information).

At last, we want to emphasize that the fast exciton trapping process does not degrade the valley CD selectivity observed in a helicity-resolved steady-state PL measurement. The excitons trapped by disorder are not counted due to its low radiative efficiency and longer emission wavelength in a PL measurement, so defect scattering to the trapped exciton is not an intervalley scattering process, although it degrades the PL emission efficiency at measured wavelength. The defect scattering time is attributed to the exciton decay time τ_A of the valley CD selectivity measured in steady-state PL: $\rho = 1/(1 + 2\tau_A/\tau_{AS})$ (eq 1 in ref 6). Intervalley scattering process (for example, intervalley phonon scattering) to a bright state in the other valley, however, can degrade the valley CD selectivity measured in PL and is attributed to the intervalley scattering time of τ_{AS}. In a defect scattering dominated sample (which is true in most current exfoliated natural flake of MoS_2 that is abundant with defects), the relation $\tau_A \ll \tau_{AS}$ holds, and thus $\rho \sim 1$.

The above equation of valley polarization assumes unity valley selection during the excitation. If we further consider that the valley initialization is not unity due to the presence of disorder strength under slightly off resonance excitation, the valley CD selectivity measured in a steady-state PL measurement does correlate with the disorder strength during the optical valley polarization initialization stage and strongly depends on pumping photon energy at large disorder strength as observed in the literature.[15,36] In the limit that defect scattering time is much faster than the intervalley scattering time, the degree of valley polarization that is measured in a steady-state PL is mainly determined by the valley polarization during the valley carrier initialization process. Lower degree of valley polarization from PL usually indicates larger disorder strength in the sample, which can potentially enhance the defect scattering rate and thus give shorter carrier valley lifetime in transient measurement. However, we want to clarify that different species of disorders or defects can play different roles in these processes. They may affect the valley polarization initialization or exciton trapping in different manners. These factors will complicate the relationship between transient measurement and steady-state PL, which requires further studies.

CONCLUSION

In the prospects of valleytronics application of TMDC, a high-quality sample with lower disorder strength is critical in two respects: suppressing the decay of valley CD selectivity of excitation away from K point to get better optical initialization of valley polarization, and suppressing the disorder dominated scattering to keep longer valley polarization for manipulating valley carriers. At the current stage, exfoliated monolayer WSe_2 shows much better quantum yield and valley polarized CD persists at an excitation energy far away from the vicinity of the K point.[8] This indicates much lower disorder strength compared to MoS_2. Improved sample quality can be further achieved by putting TMDC on a flat substrate such as BN[6] and using an improved growth method of monolayer TMDC for large-scale production, such as chemical vapor deposition[10] and molecular beam epitaxy. Similar dynamics measurements on such high-quality samples can potentially provide information of the valley polarization lifetime limited by intervalley phonon scattering.

In summary, our pump−probe measurement elucidates the probable important role of many-body effects in the transient reflection signal of monolayer MoS_2 due to reduced dimensionality. Helicity-resolved ultrafast dynamics measurement indicates that the disorder scattering is the dominant valley polarization relaxation channel in exfoliated monolayer MoS_2. In the presence of disorder, the valley CD selectivity relaxes quickly when excited away from the high-symmetry K and K′ valley. Thus, a resonant optical excitation is essential for valley polarization initialization in a highly disordered sample. Future improvement on sample quality with low disorder strength is desired for claimed valleytronics applications of TMDC.

EXPERIMENTAL METHODS

Sample Preparation. Monolayer MoS_2 flakes are obtained by mechanical exfoliation of a natural bulk MoS_2 crystal on a Si/285 nm SiO_2 substrate. The number of layers is identified by optical contrast in a microscope initially and confirmed by micro-photoluminescence spectroscopy

and micro-Raman spectroscopy, as shown in Supporting Information.

Helicity-Resolved Nondegenerate Ultrafast Pump−Probe Spectroscopy. In the nondegenerate ultrafast pump−probe setup, a 60 fs 250 kHz amplified Ti:sapphire laser at 800 nm is separated into two arms, both focused on a 2 mm sapphire plate to generate white light supercontinuum. Then a narrow band-pass filter is used to filter the desired pump and probe wavelengths for the pump−probe measurement. Both pump and probe photons are cross- or co-linear polarized before entering a Fresnel-Rhomb to get cross- or co-circular polarized light, which is subsequently focused onto the sample that is placed in a liquid-nitrogen-cooled cryostat for temperature control through a 40× near-infrared objective. Due to the tight depth of the focus of the high numerical aperture objective and 285 nm thick SiO_2 on silicon, the background pump−probe response from the Si substrate is negligible as measured on the substrate with no MoS_2 (see Supporting Information).The temporal resolution is about 200 fs, determined through both cross-correlation measurements and ΔR rise time. The reflected probe is collected by the same objective lens and detected by a Si photodetector after depolarizer and lock-in amplifier referenced to 5.7 kHz mechanically chopped pump. A narrow band filter at the probe wavelength is used to prevent the detection of a reflected pump. An additional notch filter center at the pump wavelength is added when the pump−probe wavelengths are close to each other. The probe spot size is estimated to be below 2 μm with a pump spot size slightly larger depending on the pump wavelength. The pump fluences are kept around 4×10^{14} photons/cm^2 with pump wavelength of 633 nm (1.964 eV). Pump-power-dependent dynamics measurement shows linear dependence with pump fluence, and this rules out the possibility that a higher order effect may dominate the transient response (see Supporting Information).

Conflict of Interest: The authors declare no competing financial interest.

Acknowledgment. The authors want to acknowledge T.B. Norris and Q. Niu for helpful discussion, and B.L. Liu and P.H. Tan for providing the exfoliated MoS_2 sample at the early stage of our experiment. This project has been supported by the National Basic Research Program of China (973 Grant Nos. 2012CB921300 and 2013CB921900), the National Natural Science Foundation of China (NSFC Grant Nos. 11274015 and 11174009), and the Specialized Research Fund for the Doctoral Program of Higher Education of China (Grant No. 20120001110066). All correspondence and requests for materials should be addressed to D. Sun.

Supporting Information Available: Sample photoluminescence and Raman characterization, additional helicity-resolved ultrafast spectroscopy figures and computational details. This material is available free of charge *via* the Internet at http://pubs.acs.org.

REFERENCES AND NOTES

1. Mak, K. F.; Lee, C.; Hone, J.; Shan, J.; Heinz, T. F. Atomically Thin MoS_2: A New Direct-Gap Semiconductor. *Phys. Rev. Lett.* **2010**, *105*, 136805.
2. Splendiani, A.; Sun, L.; Zhang, Y.; Li, T.; Kim, J.; Chim, C.-Y.; Galli, G.; Wang, F. Emerging Photoluminescence in Monolayer MoS_2. *Nano Lett.* **2010**, *10*, 1271–1275.
3. Mak, K. F.; He, K.; Lee, C.; Lee, G. H.; Hone, J.; Heinz, T. F.; Shan, J. Tightly Bound Trions in Monolayer MoS_2. *Nat. Mater.* **2013**, *12*, 207–211.
4. Ross, J. S.; Wu, S.; Yu, H.; Ghimire, N. J.; Jones, A. M.; Aivazian, G.; Yan, J.; Mandrus, D. G.; Xiao, D.; Yao, W.; *et al.* Electrical Control of Neutral and Charged Excitons in a Monolayer Semiconductor. *Nat. Commun.* **2012**, *4*, 1474.
5. Cao, T.; Wang, G.; Han, W.; Ye, H.; Zhu, C.; Shi, J.; Niu, Q.; Tan, P.; Wang, E.; Liu, B.; *et al.* Valley-Selective Circular Dichroism of Monolayer Molybdenum Disulphide. *Nat. Commun.* **2012**, *3*, 887.
6. Mak, K. F.; He, K.; Shan, J.; Heinz, T. F. Control of Valley Polarization in Monolayer MoS_2 by Optical Helicity. *Nat. Nanotechnol.* **2012**, *7*, 494–498.
7. Zeng, H.; Dai, J.; Yao, W.; Xiao, D.; Cui, X. Valley Polarization in MoS_2 Monolayers by Optical Pumping. *Nat. Nanotechnol.* **2012**, *7*, 490–493.
8. Jones, A. M.; Yu, H.; Ghimire, N. J.; Wu, S.; Aivazian, G.; Ross, J. S.; Zhao, B.; Yan, J.; Mandrus, D. G.; Xiao, D.; *et al.* Optical Generation of Excitonic Valley Coherence in Monolayer WSe_2. *Nat. Nanotechnol.* **2013**, *8*, 634–638.
9. Xiao, D.; Liu, G.-B.; Feng, W.; Xu, X.; Yao, W. Coupled Spin and Valley Physics in Monolayers of MoS_2 and Other Group-VI Dichalcogenides. *Phys. Rev. Lett.* **2012**, *108*, 196802.
10. Lee, Y.-H.; Zhang, X.-Q.; Zhang, W.; Chang, M.-T.; Lin, C.-T.; Chang, K.-D.; Yu, Y.-C.; Wang, J. T.-W.; Chang, C.-S.; Li, L.-J.; *et al.* Synthesis of Large-Area MoS_2 Atomic Layers with Chemical Vapor Deposition. *Adv. Mater.* **2012**, *24*, 2320–2325.
11. Wu, S.; Huang, C.; Aivazian, G.; Ross, J. S.; Cobden, D. H.; Xu, X. Vapor−Solid Growth of High Optical Quality MoS_2 Monolayers with Near-Unity Valley Polarization. *ACS Nano* **2013**, *7*, 2768–2772.
12. Zhan, Y.; Liu, Z.; Najmaei, S.; Ajayan, P. M.; Lou, J. Large-Area Vapor-Phase Growth and Characterization of MoS_2 Atomic Layers on a SiO_2 Substrate. *Small* **2012**, *8*, 966–971.
13. Li, X.; Cao, T.; Niu, Q.; Shi, J.; Feng, J. Coupling the Valley Degree of Freedom to Antiferromagnetic Order. *Proc. Natl. Acad. Sci. U.S.A.* **2013**, *110*, 3738–3742.
14. Korn, T.; Heydrich, S.; Hirmer, M.; Schmutzler, J.; Schuller, C. Low-Temperature Photocarrier Dynamics in Monolayer MoS_2. *Appl. Phys. Lett.* **2011**, *99*, 102109–102103.
15. Lagarde, D.; Bouet, L.; Marie, X.; Zhu, C.R.; Liu, B.L.; Amand, T.; Urbaszek, B. Carrier and Polarization Dynamics in Monolayer MoS_2. **2013**, *arXiv:1308.0696*.
16. Shi, H.; Yan, R.; Bertolazzi, S.; Brivio, J.; Gao, B.; Kis, A.; Jena, D.; Xing, H. G.; Huang, L. Exciton Dynamics in Suspended Monolayer and Few-Layer MoS_2 2D Crystals. *ACS Nano* **2012**, *7*, 1072–1080.
17. Wang, R.; Ruzicka, B. A.; Kumar, N.; Bellus, M. Z.; Chiu, H.-Y.; Zhao, H. Ultrafast and Spatially Resolved Studies of Charge Carriers in Atomically Thin Molybdenum Disulfide. *Phys. Rev. B* **2012**, *86*, 045406.
18. Kumar, N.; He, J.; He, D.; Wang, Y.; Zhao, H. Charge Carrier Dynamics in Bulk MoS_2 Crystal Studied by Transient Absorption Microscopy. *J. Appl. Phys.* **2013**, *113*, 133702–133706.
19. Sim, S.; Park, J.; Song, J.-G.; In, C.; Lee, Y.-S.; Kim, H.; Choi, H. Exciton Dynamics in Atomically Thin MoS_2: Inter-Excitonic Interaction and Broadening Kinetics. **2013**, *arXiv:1308.2023*.
20. Sallen, G.; Bouet, L.; Marie, X.; Wang, G.; Zhu, C. R.; Han, W. P.; Lu, Y.; Tan, P. H.; Amand, T.; Liu, B. L.; *et al.* Robust Optical Emission Polarization in MoS_2 Monolayers through Selective Valley Excitation. *Phys. Rev. B* **2012**, *86*, 081301.
21. Bromley, R. A.; Murray, R. B.; Yoffe, A. D. The Band Structures of Some Transition Metal Dichalcogenides. III. Group VIA: Trigonal Prism Materials. *J. Phys. C: Solid State Phys.* **1972**, *5*, 759–778.
22. Kasowski, R. V. Band Structure of MoS_2 and NbS_2. *Phys. Rev. Lett.* **1973**, *30*, 1175–1178.
23. Coehoorn, R.; Haas, C.; de Groot, R. A. Electronic Structure of $MoSe_2$, MoS_2, and WSe_2. II. The Nature of the Optical Band Gaps. *Phys. Rev. B* **1987**, *35*, 6203–6206.
24. Coehoorn, R.; Haas, C.; Dijkstra, J.; Flipse, C. J. F.; de Groot, R. A.; Wold, A. Electronic Structure of $MoSe_2$, MoS_2, and WSe_2. I. Band-Structure Calculations and Photoelectron Spectroscopy. *Phys. Rev. B* **1987**, *35*, 6195–6202.
25. Kadantsev, E. S.; Hawrylak, P. Electronic Structure of a Single MoS_2 Monolayer. *Solid State Commun.* **2012**, *152*, 909–913.
26. Wu, S.; Ross, J. S.; Liu, G.-B.; Aivazian, G.; Jones, A.; Fei, Z.; Zhu, W.; Xiao, D.; Yao, W.; Cobden, D.; *et al.* Electrical Tuning of Valley Magnetic Moment through Symmetry Control in Bilayer MoS_2. *Nat. Phys.* **2013**, *9*, 149–153.
27. Livescu, G.; Miller, D. A. B.; Chemla, D. S.; Ramaswamy, M.; Chang, T. Y.; Sauer, N.; Gossard, A. C.; English, J. H. Free Carrier and Many-Body Effects in Absorption Spectra of

Modulation-Doped Quantum Wells. *IEEE J. Quantum Electron.* **1988**, *24*, 1677–1689.
28. Tränkle, G.; Leier, H.; Forchel, A.; Haug, H.; Ell, C.; Weimann, G. Dimensionality Dependence of the Band-Gap Renormalization in Two- and Three-Dimensional Electron−Hole Plasmas in GaAs. *Phys. Rev. Lett.* **1987**, *58*, 419–422.
29. Schlaad, K. H.; Weber, C.; Cunningham, J.; Hoof, C. V.; Borghs, G.; Weimann, G.; Schlapp, W.; Nickel, H.; Klingshirn, C. Many-Particle Effects and Nonlinear Optical Properties of GaAs/(Al,Ga)As Multiple-Quantum-Well Structures under Quasistationary Excitation Conditions. *Phys. Rev. B* **1991**, *43*, 4268–4275.
30. Wang, H.; Shah, J.; Damen, T. C.; Pierson, S. W.; Reinecke, T. L.; Pfeiffer, L. N.; West, K. Carrier-Distribution-Dependent Band-Gap Renormalization in Modulation-Doped Quantum Wells. *Phys. Rev. B* **1995**, *52*, R17013–R17016.
31. Kleinman, D. A.; Miller, R. C. Band-Gap Renormalization in Semiconductor Quantum Wells Containing Carriers. *Phys. Rev. B* **1985**, *32*, 2266–2272.
32. Tränkle, G.; Lach, E.; Forchel, A.; Scholz, F.; Ell, C.; Haug, H.; Weimann, G.; Griffiths, G.; Kroemer, H.; Subbanna, S. General Relation between Band-Gap Renormalization and Carrier Density in Two-Dimensional Electron−Hole Plasmas. *Phys. Rev. B* **1987**, *36*, 6712–6714.
33. Ryan, J. C.; Reinecke, T. L. Band-Gap Renormalization of Optically Excited Semiconductor Quantum Wells. *Phys. Rev. B* **1993**, *47*, 9615–9620.
34. Knox, W. H.; Fork, R. L.; Downer, M. C.; Miller, D. A. B.; Chemla, D. S.; Shank, C. V.; Gossard, A. C.; Wiegmann, W. Femtosecond Dynamics of Resonantly Excited Excitons in Room-Temperature GaAs Quantum Wells. *Phys. Rev. Lett.* **1985**, *54*, 1306–1309.
35. Aaviksoo, J.; Kuhl, J. Transient Reflection of Light Near Excitonic Resonances. *IEEE J. Quantum Electron.* **1989**, *25*, 2523–2527.
36. Kioseoglou, G.; Hanbicki, A. T.; Currie, M.; Friedman, A. L.; Gunlycke, D.; Jonker, B. T. Valley Polarization and Intervalley Scattering in Monolayer MoS_2. *Appl. Phys. Lett.* **2012**, *101*, 221907.
37. Doolen, R.; Laitinen, R.; Parsapour, F.; Kelley, D. F. Trap State Dynamics in MoS_2 Nanoclusters. *J. Phys. Chem. C* **1998**, *102*, 3906–3911.